haematologica
Journal of the Ferrata Storti Foundation

Phenotypic evolution of circulating plasma cells from early precursor stages to multiple myeloma

by Martin Pietzsch, Sina Alexandra Beer, Lucca Marco Kimmich, Chiara Windsor, Sarah Gekeler, Britta Besemer and Anna Maria Paczulla Stanger

Received: October 26, 2025.
Accepted: March 11, 2026.

Citation: Martin Pietzsch, Sina Alexandra Beer, Lucca Marco Kimmich, Chiara Windsor, Sarah Gekeler, Britta Besemer and Anna Maria Paczulla Stanger. Phenotypic evolution of circulating plasma cells from early precursor stages to multiple myeloma.
Haematologica. 2026 Apr 2. doi: 10.3324/haematol.2025.300105 [Epub ahead of print]

Phenotypic evolution of circulating plasma cells from early precursor stages to multiple myeloma

Martin Pietzsch[1]*, Sina Alexandra Beer[1]*, Lucca Marco Kimmich[1], Chiara Windsor[1], Sarah Gekeler[1], Britta Besemer[1], Anna Maria Paczulla Stanger[1,2]

Author affiliations:

[1] University Clinic Tübingen, Department for Internal Medicine II, University of Tübingen, Tübingen, Germany

[2] Flow Cytometry Core Facility, Medical Faculty Tübingen, University of Tübingen, Tübingen, Germany

* These authors contributed equally to this work and share first authorship.

Key words: Multiple Myeloma, MGUS, SMM, CTPCs, disease evolution

Short title: Phenotypic evolution of CTPC in myeloma progression

Corresponding author:

Anna Maria Paczulla Stanger, PhD, Flow Cytometry Core Facility, Medical Faculty Tübingen, Otfried-Mueller-Str.10, 72076 Tübingen, Germany,

E-mail: Anna.Stanger@med.uni-tuebingen.de

ACKNOWLEDGEMENTS

We thank all participants for donating blood. We would also like to thank Prof. Dr. Claudia Lengerke and all the hospital staff who supported our study. Moreover, we thank all members of the Flow Cytometry Core Facility at the University Hospital Tübingen. This project received funding by the Nachwuchsgruppenprogramm of the Medical Faculty Tübingen to AMPS.

Figure 1 was created in BioRender (Stanger, A. (2026) https://BioRender.com/xn04d8n). We acknowledge support by Open Access Publishing Fund of University of Tübingen.

AUTHORSHIP CONTRIBUTIONS

SAB and AMPS designed the study. AMPS designed the experiments. SAB, AMPS, MP and LMK analysed and interpreted the data. LMK, SG and CW performed experiments. SAB and MP prepared the manuscript. BB supported in data analysis and correlation with clinical data. All contributing authors collected and curated data, revised and approved the manuscript.

CONFLICTS OF INTEREST

B.B. reports ad hoc reviewing activities for Janssen-Cilag and has received honoraria from Janssen-Cilag, GSK, Amgen, Sanofi, Takeda, Pfizer, and Oncopeptides. The other authors declare no conflict of interest. All authors have read and agreed to the published version of the manuscript.

DATA AVAILABILTY STATEMENT

Data are available on request from the corresponding author, Anna Stanger (anna.stanger@med.uni-tuebingen.de).

ABSTRACT

Circulating tumour plasma-cells (CTPCs) have emerged as valuable diagnostic and prognostic marker in multiple myeloma (MM), with their presence linked to progression from precursor stages and poorer outcomes in newly diagnosed MM (NDMM). While quantitative CTPC enumeration is increasingly validated, comprehensive phenotypic profiling across disease stages remains lacking. We applied 36-parameter spectral flow cytometry to 113 PBMC samples of MGUS (n=42), SMM (n=22), NDMM (n=15), treated MM (n=24), and healthy controls (n=10), alongside paired bone marrow (BM) samples from six NDMM patients. CTPCs were defined phenotypically as $CD45^{-}CD38^{high}CD56^{+}$ events without assessment of clonality. Phenotypic profiling of the $CD56^{+}$ CTPC-like subset across disease stages revealed alterations in canonical and lineage-atypical surface markers. Progression to NDMM was characterised by upregulation of CD38 and CD56 with concomitant loss of B- (CD19), myeloid- (CD14, CD16), and T-cell-associated (CD45RA) markers. In addition, HLA-ABC, interleukin receptor subunits (CD25, CD123), and chemokine receptors (CCR6, CCR7) were upregulated in NDMM. In treated MM, a reversed pattern was observed with lower CD25 and CD123 expression and increased levels of exhaustion markers (TIGIT, PD-1). Paired BM samples showed a different tissue-residency marker expression, characterised by higher CD69 and CCR6 and lower CD138, along with changes in cell-survival related markers, including increased CD25 and CD123. Both BCMA and CD307e were more highly expressed on BM plasma-cells than CTPCs. This study is among the first to provide a comprehensive phenotypic characterisation of $CD56^{+}$ CTPCs across the MM spectrum, including checkpoint and chemokine receptors, treated disease cases, and paired BM samples for NDMM.

INTRODUCTION

Multiple myeloma (MM) is a plasma cell dyscrasia characterised by the clonal proliferation of malignant plasma cells (PCs) within the bone marrow (BM), leading to abnormal immunoglobulin production and progressive skeletal destruction. In most cases, MM evolves from precursor conditions such as monoclonal gammopathy of undetermined significance (MGUS) and smouldering MM (SMM), which can persist for years before overt malignancy develops [1,2].

Disease progression is likely driven by a dynamic crosstalk between malignant PCs and the tumour microenvironment (TME), promoting sub-clonal evolution as well as invasion across various BM niches and beyond [3]. In long-standing precursor lesions, chronic immune activation likely exposes the immune system to tumour-associated neoantigens over many years, leading to immune dysfunction and T-cell exhaustion [3,4]. However, the underlying biology including the timely pattern of disease progression remains poorly understood. Current risk-stratification models, despite recent advances, still have limitations in predicting which patients with MGUS or SMM will progress to symptomatic MM [5,6], underscoring the need for more precise biomarkers.

Circulating tumour plasma cells (CTPCs) have emerged as a powerful diagnostic and prognostic tool in MM. Using spectral flow cytometry (SFC), CTPCs can be detected in the peripheral blood (PB) of virtually all newly diagnosed MM (NDMM) patients and, depending on assay sensitivity, reliably identified in precursor conditions [7]. Their presence is associated with progression in MGUS and SMM and is linked to poorer outcomes in NDMM, although definitive cut-offs still need to be established [8,9]. Interestingly, high CTPC counts are observed to be associated with a distinct immune profile in both PB and TME (e.g., higher levels of cytotoxic T-/NK-cells and tumour-associated macrophages, increased memory/naive B-cell ratio) [10,11]. Yet, while quantitative CTPC enumeration is increasingly validated, comprehensive phenotypic profiling of CTPCs themselves across disease stages is lacking.

In this study, we leveraged high-parameter spectral flow cytometry in a real-world cohort of MGUS, SMM, NDMM, and treated MM patients to delineate CTPC phenotypic evolution across disease stages. Our aim was to uncover biomarkers in precursor conditions and advance our understanding of myeloma biology.

METHODS

Study population and clinical data acquisition. We conducted a cross-sectional study including adult patients with MGUS, SMM, NDMM or treated MM in an outpatient care setting at the department of Internal Medicine II, University Hospital Tübingen. From 02/22 - 07/23, we obtained peripheral blood mononuclear cell (PBMC) samples from 103 patients, who met flow cytometry quality control criteria (i.e., sufficient viable cell counts for staining and measurement, CPC count over limit of detection) and study inclusion criteria (**Figure 1**). Six matched BM aspirates of NDMM patients were collected. Ten fully anonymised healthy blood-bank donors served as controls.

For MGUS, SMM and MM patients, electronic medical records were reviewed regarding disease subtype, therapy lines, remission status (defined based on the international myeloma working group (IMWG) criteria), and laboratory findings. Risk stratification was performed using the Mayo Clinic MGUS Risk Stratification Model [12], the IMWG 2/20/20 model for SMM [6], and the updated IMS/IMWG high-risk guidelines for MM patients [13].

Analysis of Multiparameter spectral flow-cytometry. PB mononuclear cells (PBMCs) were enriched by density gradient centrifugation and viably frozen.

Single cell suspensions from PBMCs of patients were stained with fluorescently labelled antibodies (see **Supplementary Table 1** and Supplementary Material for more details). For spectral unmixing, a combination of both single stained cells and UltraComp eBeads™ Plus Compensation Beads (ThermoFisher) was applied. Dead cells were excluded using LIVE/DEAD™ Fixable Blue Dead Cell Staining dye (ThermoFisher). The panel and gating strategy were adapted from the OMIP-069 immunophenotyping protocol [14]. Samples were acquired using a Cytek AURORA spectral flow cytometer enabling simultaneous detection of all cell types and qualitative markers. Analysis was performed with Cytolution Software (from Cytolytics GmbH) using manual gating as shown in **Supplementary Figure 1** for B cells and PCs with subsequent cluster exploration to analyse mean fluorescence intensity (MFI) values across each cellular subset. A more detailed description can be found in the Supplementary information.

CPCs were identified by a $CD45^{-}CD38^{high}$ immunophenotype. CD56 expression was subsequently used to identify aberrant CPCs (i.e., $CD56^{+}$ CTPCs), as CD56 represents one of the most consistently altered markers in clonal plasma cells [15]. Light chain clonality (κ/λ) and additional markers included in the EuroFlow NGF panel, such as CD27 or CD81, were not

primarily used to gate CTPCs. The limit of detection was set at ≥ 20 CPC events, and samples below this threshold were excluded from marker expression analyses.

Ethics and informed consent. The study was approved by the institutional Ethical Committees in accordance with the Declaration of Helsinki (no. 161/2022B02). All patients and controls provided informed consent before study inclusion.

Statistical analysis. Statistical analyses were performed using GraphPad Prism (v10.5.0). Comparisons were performed after analysis of normal distribution using the Anderson-Darling test. Continuous variables were analysed using Welch's t-test, paired t-test, Mann-Whitney test or Wilcoxon rank-sum tests as appropriate. We performed ANOVA (normally distributed) or Kruskal-Wallis (K-W, nonparametric) to investigate differences in > 2 groups, with adjustment for multiple comparisons by post hoc Benjamini, Krieger & Yekutieli procedure for false discovery rate (FDR) correction. Desired FDR Q was set at 0.05. Test-specific effect sizes were reported for all analyses, with 95% confidence intervals where applicable. All tests were two-sided, and *P*-values < 0.05 were considered significant. In case of FDR correction, adjusted *P*-values (q values) of < 0.05 were considered a statistically significant discovery.

RESULTS

Patient and treatment characteristics. 103 patients were included in the analysis, of which 42 (40.7%) had MGUS, 22 (21.4%) SMM, 15 (14.6%) NDMM and 24 (23.3%) treated MM at sample collection (**Figure 1**). In addition to PBMCs, paired BM samples were available for six of 15 NDMM patients (40.0%). Clinical baseline and treatment characteristics are summarized in **Table 1**. Mean interval from initial diagnosis to sample collection was 60.2 months (interquartile range [IQR] 13.8 – 78.3) for MGUS, 53.0 months (IQR 14.0 – 89.3) for SMM, 1.0 month (IQR 0.0 – 1.0) for NDMM and 60.0 months for treated MM (IQR 36.3 – 77.3). All subsequent results are presented with reference to PBMCs unless otherwise specified and focus on differences between MGUS, SMM and NDMM in comparison to healthy controls.

B cell counts and disease progression. The percentage of total B cells ($CD19^+$) of all $CD45^+$ cells in PB did not significantly differ between healthy controls (mean 10.43%, standard deviation (SD) 2.20), MGUS (mean 10.77%, SD 4.45), SMM (mean 9.93%, SD 5.64) and NDMM (11.27%, SD 7.01). However, a relevant subset of MGUS (33%), SMM (50%) and MM patients (40%) had reduced B-cell proportions compared to healthy controls (**Figure 2a**). Moreover, subset analysis revealed distinct changes in the composition of the B-cell compartment with disease progression. The percentage of naive B-cells in MGUS (67.65%) and SMM (65.94%) did not differ from healthy controls (67.46%) (Healthy vs. MGUS adj. *P* =

0.851, Healthy vs. SMM adj. *P* = 0.837), whereas a marked drop in naive B-cells was seen in NDMM (55.16%) compared to MGUS (adj. *P* = 0.036, Hedges' g = 0.84, 95% CI [0.21, 1.46]) and SMM (adj. *P* = 0.089, Hedges' g = 0.63, 95% CI [0.02, 1.24]) (**Figure 2b**). Switched and unswitched memory B-cells were lower in MGUS (8.79% and 4.08%, respectively) and SMM (6.58% and 2.92%, respectively) compared to healthy levels (11.07% and 8.31%; Healthy vs. SMM adj. *P* = 0.013 for unswitched, r_{rb} = 0.41) but significantly higher in NDMM (16.84% and 11.50%; NDMM vs. MGUS adj. *P* = 0.004, r_{rb} = 0.43 and NDMM vs. SMM adj. *P* < 0.001, r_{rb} = 0.61 for switched; NDMM vs. MGUS adj. *P* < 0.001, r_{rb} = 0.53 and NDMM vs. SMM adj. *P* < 0.001, r_{rb} = 0.71 for unswitched) (**Figure 2b**). Conversely, a trend toward higher levels of translational B-cells in MGUS (4.15%) and SMM (4.04%) was seen compared to NDMM (2.21%), yet this trend did not reach statistical significance (NDMM vs. MGUS/SMM both *P* = 0.065). No differences were found for plasmablast counts in PB (**Figure 2b**).

CPC and CTPC counts and disease progression. $CD56^-$ CPCs could be found in 100% of healthy donors with a median of 44.6/100.000 cells. They were slightly lower in MGUS (median 37.2/100.000 cells) and SMM (37.7/100.000 cells) but comparable to healthy levels in NDMM (median 48.7/100.000 cells) (**Figure 3a**). The median number of $CD56^+$ circulating tumour plasma cells (CTPCs) rose significantly from MGUS (2.54, IQR 1.13 – 7.18) to SMM (6.96, IQR 2.66 – 13.89) to NDMM (median 16.34, IQR 12.86 – 86.78) (overall *P* < 0.001, ε^2 = 0.17) (**Figure 3b**). For the whole CPC compartment in the PB, this translated into a significantly increased median percentage of $CD56^+$ CTPCs from MGUS (5.62%), to SMM (13.01%) and NDMM (32.41%) (overall *P* = 0.002, ε^2 = 0.20) (**Figure 3c**). Plasma cells with aberrant CD56 expression were also found in healthy donors, albeit at lower frequencies compared to precursor states and NDMM (median 1.9/100.000 cells, IQR 0.49 - 3.84, median percentage of all CPCs 3.65%, **Figure 3b and c**).

Exploratorily, we categorised all samples into "CTPC high" ($\geq$ 0.02%) and "CTPC low" (< 0.02%) by using a threshold established by Kostopoulos et al [16] for CTPC enumeration by Next-Generation-Flow (NGF). Classified as "CTPC high" were 9.5% (4/42) of MGUS, 18.2% (4/22) of SMM and 40.0% (6/15) of NDMM (**Figure 3d**). Acknowledging the cohort size in our study as well as the use of a SFC, we did not observe any clear correlations between "CTPC high" and advanced risk scores for MGUS and SMM cases. Among the six NDMM samples classified as "CTPC high", two patients were also classified as IMS/IMWG high-risk (33.3%). All "CTPC low" NDMM samples had standard-risk according to IMS/IMWG criteria, except one classified as high-risk due to elevated β2-microglobulin with additional gain1q21. When applying a less stringent threshold of 2% of nucleated cells for classification as "CTPC high", none of the patients in our groups met this criterion.

CTPC phenotype profiles. CTPC phenotypic profiling was based using a total of 36 parameters (**Supplementary Table 1)**, with CTPCs phenotypically defined as $CD45^{-}$ $CD38^{high}CD56^{+}$ events, whilst clonality was not assessed. Therefore, the findings reflect the $CD56^{+}$ CTPC-like subset. CPCs from healthy controls served as comparison. Across disease progression from MGUS and SMM to NDMM, $CD56^{+}$ CTPCs showed distinct changes in marker expression, including aberrant expression of markers not typically expected with the CTPC phenotype. All *P*-values for each marker and comparison are provided in **Supplementary Table 2**, and boxplots for each marker are shown in **Supplementary Figure 2**.

B- and plasma-cell related markers on CTPCs across disease stages

Consistent with normal PC maturation, $CD56^{+}$ CTPCs showed increasing CD38 expression accompanied by loss of CD19 expression across disease stages, reaching the highest CD38 levels (according to its mean fluorescence intensity, MFI) in NDMM. CD27 levels were consistently lower compared to healthy PCs. CD138 and BCMA expression remained stable across MGUS, SMM, and NDMM, whereas CD307e was significantly upregulated in SMM and NDMM compared to MGUS (both adj. $P < 0.01$, $r_{rb} = 0.34$ and 0.59) (**Figure 4a**). Although, particularly in MGUS, wide interpatient variability was observed. CD20 showed no clear pattern across stages; however, the highest levels in NDMM were observed in a patient with t(11;14). Interestingly, even though CTPCs were defined as CD45 negative, the CD45RA isoform showed robust expression in MGUS, whereas levels were lowest in NDMM (overall $P < 0.001$, $\eta^2 = 0.41$, 95 % CI [0.23, 0.55]) (**Figure 4b and g, Supplementary Figure 4**).

T- and myeloid-cell related markers on CTPCs across disease stages

While CD3 expression on plasma cells was mutually exclusive with CD56 in our data, resulting in the absence of $CD3^{+}$ CTPCs (data not shown), several T-cell associated markers were aberrantly expressed on $CD56^{+}$ CTPCs despite the lack of CD3 expression. CD4 expression declined in MGUS samples but showed no further significant changes in SMM and NDMM relative to healthy PCs. In contrast, CD8 expression on CTPCs seemed to robustly increase from precursor states to NDMM (overall $P < 0.001$, $\varepsilon^2 = 0.36$) (**Figure 4c**). In cross-sectional comparison, expression of the interleukin (IL) receptor subunits CD25/IL-2RA and CD123/IL-3RA were lower in MGUS and SMM than in healthy controls, but again equally expressed in NDMM (CD25: overall $P < 0.001$, $\varepsilon^2 = 0.22$; CD123: overall $P < 0.001$, $\varepsilon^2 = 0.29$) (**Figure 4d and h**). In contrast to IL receptor subunits, the myeloid-related cell markers CD14 and CD16 were highest expressed on $CD56^{+}$ CTPCs in MGUS, followed by a lower expression across subsequent disease stages (CD14: overall $P = 0.010$, $\varepsilon^2 = 0.10$; CD16: overall $P = 0.001$, $\varepsilon^2 = 0.15$) (**Figure 4d)**.

Activation, checkpoint, and chemokine receptor signatures on CTPCs across disease stages

We next assessed aberrant expression of activation signatures on $CD56^+$ CTPCs. The activation marker CD69 showed declining levels from MGUS over SMM to NDMM samples, with the lowest MFI observed in NDMM (overall P <0.001, $\varepsilon^2 = 0.34$) (**Figure 4e**). In contrast, HLA-DR and HLA-ABC expression, reduced in MGUS and SMM, reached levels comparable to those in healthy controls in NDMM (**Figure 4b**). Among checkpoint molecules, TIM-3 expression on $CD56^+$ CTPCs showed a trend toward upregulation in NDMM compared to MGUS and SMM, although this did not reach statistical significance (NDMM vs. MGUS/SMM: both adj. $P = 0.103$, $r_{rb} = 0.17$ and 0.38), whereas PD-1 and TIGIT showed the opposite pattern, with significant lower expression in SMM and NDMM (NDMM vs. MGUS: adj. P <0.001 for PD-1, $r_{rb} = 0.59$; $P = 0.002$ for TIGIT, $r_{rb} = 0.48$) (**Figure 4e and i**).

Interestingly, the chemokine receptors CCR6 and CCR7 were elevated in NDMM compared to all other groups, with CCR7 showing a particularly pronounced increase (CCR6: NDMM vs. MGUS/SMM adj. $P < 0.01$, $r_{rb} = 0.39$ and 0.50; CCR7: NDMM vs. MGUS/SMM adj. P <0.001, $r_{rb} = 0.60$ and 0.67) (**Figure 4f and j**). The expression of CCR4 remained stable across disease stages and was comparable to MFIs on CPCs from healthy donors.

CTPC phenotypes in the treated MM cohort

In the treated MM cohort (n=24), a mostly reversed pattern compared to the disease evolution from MGUS, SMM to NDMM could be observed. Compared to NDMM, $CD56^+$ CTPCs displayed a significant lower expression of CD38 (P <0.001, $r_{rb} = 0.73$) and CD56 ($P = 0.001$, $r_{rb} = 0.62$) as well as a significant regain of CD19 ($P = 0.006$, $r_{rb} = 0.52$) and CD45RA (P <0.001, Hedges' g = 1.79, 95% CI [1.05, 2.58]) after treatment (**Figure 5a-c**). Interestingly, CD307e expression was significantly lower in the treated cohort (P <0.001, $r_{rb} = 0.76$), whereas the expression of BCMA increased compared to NDMM ($P = 0.020$, Hedges' g = 0.67, 95% CI [0.02, 1.35], **Figure 5b**). Of note, only one of our treated patients received BCMA-directed therapy (**Table 1**) and this patient did show a comparable BCMA expression to other samples without BCMA-directed therapy.

The MFI of T-cell related markers such as CD4 and CD8 significantly decreased post-treatment compared to NDMM ($P < 0.001$, Hedges' g = 1.02, 95% CI [0.34, 1.72], and P <0.001, Hedges' g = 1.52, 95% CI [0.81, 2.28], respectively). Moreover, the expression of the IL receptor subunits CD25 ($P < 0.001$, $r_{rb} = 0.81$) and CD123 ($P = 0.003$, Hedges' g = 0.93, 95% CI [0.26, 1.62]) was significantly lower in the treated cohort compared to NDMM (**Figure 5d**). Checkpoint and chemokine receptor expression appeared to recover after treatment. Although based on

a cross-sectional setting, the trends were striking, with PD-1 (P <0.001, r_{rb} = 0.78) and TIGIT (P = 0.003, r_{rb} = 0.56) increasing and TIM-3 (P = 0.002, r_{rb} = 0.78), CCR6 (P = 0.192, r_{rb} = 0.26) and CCR7 (P = 0.004, r_{rb} = 0.55) decreasing again compared to NDMM (**Figure 5e and f**).

CTPC phenotypes compared to BM PC phenotypes in NDMM

For six patients with NDMM paired PB and BM samples were available, which were further analysed regarding phenotypic differences. The six combined samples presented with similar differences when comparing PB and BM (**Supplementary Figure 3**). Whereas CD69 expression was low on $CD56^+$ CTPCs in NDMM, bone marrow plasma cells (BMPCs) exhibited markedly higher CD69 levels (P = 0.013, d_z = 1.55, 95% CI [0.68, 4.16]), potentially in analogy to its role in tissue residency in T cells (**Figure 6a**). Conversely, $CD56^+$ CTPCs showed a significantly higher expression of CD138 (**Figure 6a**) than their BM counterparts (P = 0.002, d_z = 2.48, 95% CI [0.77, 4.15]), whereas expression of CD14 (P = 0.007, d_z = 1.77, 95% CI [0.42, 3.08]), CD25 (P = 0.009, d_z = 1.67, 95% CI [0.77, 4.45]) and CD123 (P = 0.017, d_z = 1.44, 95% CI [0.59, 3.93], **Figure 6a and b, Suppl. Figure 3**) was significantly lower on $CD56^+$ CTPCs. Interestingly, BCMA and, in particular, CD307e expression were significantly higher on BMPCs than on $CD56^+$ CTPCs (P = 0.049, d_z = 1.06, 95% CI [0.01, 2.05] and P = 0.002, d_z = 2.53, 95% CI [1.37, 6.48], respectively) (**Figure 6c**). CD8 showed a markedly higher expression on BMPC compared to $CD56^+$ CTPCs in all samples (P = 0.002, d_z = 2.38, 95% CI [1.29, 6.10]) (**Figure 6b**). Finally, CCR6 was significantly lower expressed on $CD56^+$ CTPCs than on BMPCs (P = 0.037, d_z = 1.15, 95% CI [0.06, 2.18]), whereas no differences were observed for CCR4 and CCR7, possibly reflecting the distinct chemokine milieu in PB (**Figure 6d**).

DISCUSSION

In this study, we used multi-dimensional spectral flow cytometry with a 33-marker (36 parameter) panel in a cohort of MGUS, SMM, NDMM, and treated MM patients to delineate B-cell and $CD56^+$ CTPC phenotypes across disease stages and after treatment.

Using this technique, we showed no significant differences regarding absolute B-cell counts and subset distributions in PB between MGUS patients and healthy controls. However, NDMM samples were marked by higher levels of switched and unswitched memory B-cells compared to precursor stages as well as a drop in naive B-cell counts. The observation of increased memory B-cells is consistent with previous studies [17,18], and has led to speculation about possible “myeloma-initiating” or MM stem cells among the circulating memory B-cell population [18,19]. Furthermore, it has been shown that MM cells in relapse seem to emerge from a pool of

progenitor cells found among B-cells [20], highlighting the necessity of further investigation into the relationship between B-cells and MM cells.

Analyses of relative and absolute CD56$^+$ CTPC counts demonstrated stepwise increases from MGUS to SMM to NDMM, as reported before [21]. After exploratorily classifying all samples into "CTPC high" (> 0.02%) and "CTPC low" (< 0.02%) by using a binary threshold analogous to Kostopoulos et al [16], we did not observe strong overlap with established risk stratification models in precursor stages. For NDMM, virtually all CTPC-low cases (8/9, 89%) were classified as standard risk by the updated IMS/IMWG HR guidelines. Interestingly, a gain or amplification of 1q21 was present in 4 of 6 (66.7%) CTPC-high samples, but only in 2 out of 9 (22.2%) CTPC-low samples. This observation confirms a trend priorly seen for CTPCs in AL amyloidosis [22]. However, comparisons with risk models remain underpowered due to cohort size and may not be directly transferable due to different gating strategies.

The CD56$^+$ CTPC phenotypes showed maturation-consistent changes across disease stages in B-cell and PC markers. This was surprisingly accompanied by acquisition of various T-cell and myeloid-related features not typically associated with CPCs. Notably, NDMM samples could be well distinguished from healthy controls, MGUS and SMM by several specific expression patterns. First, they showed a more terminally differentiated and malignant PC phenotype than MGUS and SMM samples. CD38 and CD56 expressions were highest, while CD19, CD27, and CD45RA were lower expressed. Interestingly, CD20 expression was highest in NDMM with t(11;14), consistent with this translocation being associated with a more B-cell-like phenotype [23]. Second, the antigen presentation machinery via HLA-ABC and HLA-DR appeared to be altered in NDMM. HLA-ABC, reduced in MGUS and SMM, reached comparable high levels to healthy controls, potentially pointing to an advanced tumour stage with activated immune microenvironment as it is seen in breast cancer cells expressing HLA-ABC [24]. Third, non-canonical markers expressed on CTPCs suggest a potentially modified checkpoint and survival-signalling profile in NDMM. Specifically, PD-1 and TIGIT were lower, but TIM-3 levels were higher on NDMM CD56$^+$ CTPCs compared to MGUS and SMM samples. Given its inhibitory role known from tumour-infiltrating lymphocytes [25], elevated TIM-3 expression on CTPCs warrants future functional validation to determine whether TIM-3 plays a biological role in CTPC persistence in peripheral blood. Furthermore, several IL receptor subunits (CD25/IL-2RA, CD123/IL-3RA) were lower on CTPCs in MGUS and SMM than in healthy controls but higher in NDMM. Among others, they activate STAT5, which has been linked to suppression of anti-tumour immunity and enhanced tumour cell survival [26]. This pattern would be consistent with increased cytokine responsiveness and pro-survival signalling in advanced MM disease [27]. Compared with BMPCs, CD25 and CD123 were lower on CD56$^+$

CTPCs (both $P < 0.01$), possibly suggesting niche-specific survival programs. In line with our findings, the BM of MM patients has been shown to be enriched for IL-3 and interactions between plasmacytoid dendritic cells and BMPC might further support this signalling axis [28,29]. As our panel identified CTPCs without clonality assessment, we acknowledge that non-canonical marker patterns may also occur on reactive, polyclonal plasma cells that transiently express CD56.

Notably, CCR6 and CCR7 were significantly elevated on $CD56^+$ CTPCs in NDMM compared to all other groups, suggesting potential differences in trafficking cues. CCR6 was even higher expressed on BMPCs than on matched $CD56^+$ CTPCs ($P = 0.037$), in line with reports that malignant PC upregulate CCR6 in their TME and promote osteolytic bone disease [30]. This modified chemokine signature could relate to extramedullary disease (EMD), as a correlation between CCR7 expression on BMPC and EMD has already been shown [31]. Unfortunately, our cohort contained too few patients with EMD at sampling to draw a robust connection. Lastly, the activation marker CD69 was lower in NDMM samples, potentially in analogy to its role in tissue residency in memory T cells [32]. This aligns with higher CD69 levels on BMPCs than on matched CTPCs.

In the treated MM cohort, the described NDMM-associated phenotypic changes were partially or fully normalised. The significant lower CD38 expression post-treatment may reflect either disease remission or antigen escape secondary to anti-CD38 therapy [33]. Moreover, the higher expression of CD19 post treatment could represent the accumulation of less-differentiated PC subclones after therapy-induced pressure [34].

Given their therapeutic relevance, we assessed BCMA and CD307e expression across disease stages. BCMA on $CD56^+$ CTPCs did not differ meaningfully between MGUS, SMM, and NDMM, with slightly higher levels after treatment. This finding was unlikely to be influenced by BCMA-directed therapies in our cohort, as only one patient had received anti-BCMA CAR-T cells. In the six paired NDMM samples, BCMA expression was higher on BMPCs than on $CD56^+$ CTPCs ($P = 0.049$). CD307e was significantly increased in SMM and NDMM compared to MGUS (both $P < 0.01$) and was also higher on BMPCs than on $CD56^+$ CTPCs ($P = 0.002$). The pronounced expression in SMM samples may warrant evaluation as a therapeutic target specifically in this precursor state, however, validation in larger cohorts is essential.

Limitations of this study include the cross-sectional design and limited per-group sample sizes, particularly for matched BM samples. Although PBMC sample numbers are decent, statistical power was limited to detect robust associations with clinical features, considering also inter-patient variability in marker expression. Moreover, our CTPC gating strategy relied on CD56

expression to identify aberrant CPCs. While this approach captures the predominant malignant phenotype reported for CTPCs in MM, it likely underestimates the full CTPC compartment and may include rare non-clonal plasma cells due to non-assessed clonality. Future studies with larger, longitudinal cohorts, CTPC gating as defined in the full EuroFlow NGF panel, and functional validation will be mandatory to establish biological relevance and clinical utility of our findings. Incorporating cytogenetics could help to identify aggressive subclones [35].

Despite these limitations, this study provides one of the first comprehensive descriptions of CTPC phenotypes across disease stages and could establish a framework for further investigation. CTPC phenotyping supported by orthogonal data, such as recent single-cell transcriptomic profiling of CTPCs [36], will be essential to determine whether phenotypic features add predictive value beyond CTPC counts in discriminating progression patterns. Given its minimally invasive nature compared with BM sampling and the widespread availability of flow cytometry, this approach has the potential to deepen our understanding of progression patterns and also investigate therapeutic target availability in NDMM and treated MMs.

REFERENCES

1. Weiss BM, Abadie J, Verma P, et al. A monoclonal gammopathy precedes multiple myeloma in most patients. Blood. 2009;113(22):5418-5422.
2. Landgren O, Kyle RA, Pfeiffer RM, et al. Monoclonal gammopathy of undetermined significance (MGUS) consistently precedes multiple myeloma: a prospective study. Blood. 2009;113(22):5412-5417.
3. Dhodapkar MV. The immune system in multiple myeloma and precursor states: Lessons and implications for immunotherapy and interception. Am J Hematol. 2023;98 Suppl 2(Suppl 2):S4-S12.
4. Dang M, Han G, Lee HC, et al. Single cell clonotypic and transcriptional evolution of multiple myeloma precursor disease. Cancer Cell. 2023;41(6):1032-1047.e4.
5. Maeng CV, Rögnvaldsson S, Einarsson Long T, et al. Revised free light chain reference intervals enhance risk stratification in monoclonal gammopathy of undetermined significance and reduce overdiagnosis. Blood Cancer J. 2025;15(1):80.
6. Mateos M-V, Kumar S, Dimopoulos MA, et al. International Myeloma Working Group risk stratification model for smoldering multiple myeloma (SMM). Blood Cancer J. 2020;10(10):102.
7. Sanoja-Flores L, Flores-Montero J, Pérez-Andrés M, et al. Detection of Circulating Tumor Plasma Cells in Monoclonal Gammopathies: Methods, Pathogenic Role, and Clinical Implications. Cancers (Basel). 2020;12(6):1499.
8. Gonsalves WI, Jevremovic D, Nandakumar B, et al. Enhancing the R-ISS classification of newly diagnosed multiple myeloma by quantifying circulating clonal plasma cells. Am J Hematol. 2020;95(3):310-315.
9. Bertamini L, Grasso M, D'Agostino M, et al. Poor Prognosis of Multiple Myeloma Predicted By High Levels of Circulating Plasma Cells Is Independent from Other High-Risk Features but Is Modulated By the Achievement of Minimal Residual Disease Negativity. Blood. 2020;136(Supplement 1):12-13.
10. Kostopoulos IV, Ntanasis-Stathopoulos I, Rousakis P, et al. Circulating Plasma Cells in Newly Diagnosed Multiple Myeloma: Prognostic and More. J Clin Oncol. 2023;41(3):708-710.
11. Papadimitriou K, Tsakirakis N, Malandrakis P, et al. Deep Phenotyping Reveals Distinct Immune Signatures Correlating with Prognostication, Treatment Responses, and MRD Status in Multiple Myeloma. Cancers (Basel). 2020;12(11):3245.
12. Stern S, Chaudhuri S, Drayson M, et al. Investigation and management of the monoclonal gammopathy of undetermined significance. Br J Haematol. 2023;202(4):734-744.
13. Avet-Loiseau H, Davies FE, Samur MK, et al. International Myeloma Society/International Myeloma Working Group Consensus Recommendations on the Definition of High-Risk Multiple Myeloma. J Clin Oncol. 2025;43(24):2739-2751.
14. Park LM, Lannigan J, Jaimes MC. OMIP-069: Forty-Color Full Spectrum Flow Cytometry Panel for Deep Immunophenotyping of Major Cell Subsets in Human Peripheral Blood. Cytometry A. 2020;97(10):1044-1051.
15. Flores-Montero J, Sanoja-Flores L, Paiva B, et al. Next Generation Flow for highly sensitive and standardized detection of minimal residual disease in multiple myeloma. Leukemia. 2017;31(10):2094-2103.
16. Kostopoulos IV, Ntanasis-Stathopoulos I, Rousakis P, et al. Low circulating tumor cell levels correlate with favorable outcomes and distinct biological features in multiple myeloma. Am J Hematol. 2024;99(10):1887-1896.
17. Schinke C, Poos AM, Bauer M, et al. Characterizing the role of the immune microenvironment in multiple myeloma progression at a single-cell level. Blood Adv. 2022;6(22):5873-5883.
18. Všianská P, Říhová L, Varmužová T, et al. Analysis of B-cell subpopulations in monoclonal gammopathies. Clin Lymphoma Myeloma Leuk. 2015;15(4):e61-71.

19. Matsui W, Wang Q, Barber JP, et al. Clonogenic multiple myeloma progenitors, stem cell properties, and drug resistance. Cancer Res. 2008;68(1):190-197.
20. Tiedemann RE, Tagoug I, Erdmann N, et al. Multiple Myeloma B Cells and Pre-Plasma Cells Are Important Reservoirs for Myeloma Relapse Following Plasma Cell-Directed Therapy and Prevent Cure with Standard Therapies. Blood. 2023;142(Supplement 1):642.
21. Bertamini L, Oliva S, Rota-Scalabrini D, et al. High Levels of Circulating Tumor Plasma Cells as a Key Hallmark of Aggressive Disease in Transplant-Eligible Patients With Newly Diagnosed Multiple Myeloma. J Clin Oncol. 2022;40(27):3120-3131.
22. Kastritis E, Kostopoulos IV, Theodorakakou F, et al. Prognostic Significance of Circulating Plasma Cells Detected By Next Generation Flow Cytometry in Light (AL) Chain Amyloidosis. Blood. 2022;140(Supplement 1):1150-1151.
23. Bal S, Kumar SK, Fonseca R, et al. Multiple myeloma with t(11;14): unique biology and evolving landscape. Am J Cancer Res. 2022;12(7):2950-2965.
24. Lee HJ, Song IH, Park IA, Heo S-H, Kim Y-A, Ahn J-H, Gong G. Differential expression of major histocompatibility complex class I in subtypes of breast cancer is associated with estrogen receptor and interferon signaling. Oncotarget. 2016;7(21):30119-30132.
25. Burugu S, Gao D, Leung S, Chia SK, Nielsen TO. TIM-3 expression in breast cancer. Oncoimmunology. 2018;7(11):e1502128.
26. Rani A, Murphy JJ. STAT5 in Cancer and Immunity. J Interferon Cytokine Res. 2016;36(4):226-237.
27. Wingelhofer B, Neubauer HA, Valent P, et al. Implications of STAT3 and STAT5 signaling on gene regulation and chromatin remodeling in hematopoietic cancer. Leukemia. 2018;32(8):1713-1726.
28. Ray A, Das DS, Song Y, et al. A novel agent SL-401 induces anti-myeloma activity by targeting plasmacytoid dendritic cells, osteoclastogenesis and cancer stem-like cells. Leukemia. 2017;31(12):2652-2660.
29. Ehrlich LA, Chung HY, Ghobrial I, et al. IL-3 is a potential inhibitor of osteoblast differentiation in multiple myeloma. Blood. 2005;106(4):1407-1414.
30. Giuliani N, Lisignoli G, Colla S, et al. CC-chemokine ligand 20/macrophage inflammatory protein-3α and CC-chemokine receptor 6 are overexpressed in myeloma microenvironment related to osteolytic bone lesions. Cancer Res. 2008;68(16):6840-6850.
31. Wang YN, Gan SL, Wu FF, et al. [Expression of CC-chemokine Receptor 7 in Patiens with Multiple Myeloma and Its Relationship with Extramedullary Disease]. Zhongguo Shi Yan Xue Ye Xue Za Zhi. 2017;25(2):476-479.
32. Schneider Revueltas E, Ferreira-Gomes M, Guerra GM, et al. Surface CD69-Negative CD4 and CD8 Bone Marrow-Resident Human Memory T Cells. Eur J Immunol. 2025;55(5):e202451529.
33. Diamond BT, Baughn LB, Poorebrahim M, et al. Biallelic antigen escape is a mechanism of resistance to anti-CD38 antibodies in multiple myeloma. Blood. 2025;146(13):1575-1585.
34. Paiva B, Puig N, Cedena MT, et al. Differentiation stage of myeloma plasma cells: biological and clinical significance. Leukemia. 2017;31(2):382-392.
35. Lightbody ED, Sklavenitis-Pistofidis R, Wu T, et al. SWIFT-seq enables comprehensive single-cell transcriptomic profiling of circulating tumor cells in multiple myeloma and its precursors. Nat Cancer. 2025;6(9):1595-1611.
36. Garcés J-J, Simicek M, Vicari M, et al. Transcriptional profiling of circulating tumor cells in multiple myeloma: a new model to understand disease dissemination. Leukemia. 2020;34(2):589-603.

TABLES

Table 1: Clinical, laboratory and molecular characteristics of the study cohort. *****Samples were obtained from a blood bank and were fully anonymized. MGUS, monoclonal gammopathy of undetermined significance; SMM, smouldering multiple myeloma; NDMM, newly diagnosed multiple myeloma; ISS, international staging system; HD/ASCT, High-dose chemotherapy/autologous stem cell transplantation; CR, complete response; PR, partial response; PD, progressive disease; International Myeloma Working Group; PI, proteasome inhibitor; IMiD, immunomodulatory drug; NA, not applicable; LCO, Light chain only; N, number.

Information	**MGUS** N = 42	**SMM** N = 22	**NDMM** N = 15	**treated MM** N = 24	**Healthy controls *** N = 10
Sex, male, n (%)	20 (48)	9 (41)	7 (47)	13 (54)	*n.a.*
Age initial diagnosis, mean (range)	57.7 (33 - 86)	61.3 (35 - 79)	67.1 (41 - 87)	61.3 (43 - 81)	*n.a.*
Age at sampling, mean	62.8	65.9	67.1	66.3	
< 65 years	25	10	5	11	*n.a.*
≥ 65 years	17	12	10	13	
Haemoglobin level (g/dl) (range)	13.6 (10.1 - 15.8)	13.4 (10.2 - 15)	11.6 (8.2 - 15.5)	12.4 (8.9 - 16.3)	*n.a.*
Unknown	*5*	*0*	*0*	*0*	
B2-microglobulin (mg/l) (range)	2.3 (1.1 - 4.5)	2.3 (1.4 - 3.3)	3.8 (1.5 - 7.1)	5.5 (1.8 - 17.5)	
> 5.5, n (%)	0 (0)	0 (0)	2 (13)	6 (25)	*n.a.*
> 5.5 & creatine < 1.2mg/dl, n (%)	0 (0)	0 (0)	1 (7)	2 (8)	
Unknown	*11 (26)*	*2 (9)*	*0 (0)*	*2 (8)*	
ISS, n (%)					
1			4 (27)	5 (21)	
2	*n.a.*	*n.a.*	7 (47)	11 (46)	*n.a.*
3			4 (27)	8 (33)	
Unknown			*0 (0)*	*0 (0)*	
IMS/IMWG-HR (consensus 2025), n (%)					
Standard-risk	*n.a.*	*n.a.*	11 (73)	15 (62)	*n.a.*
High-risk			3 (20)	4 (17)	
Unknown			*1 (7)*	*5 (21)*	
MGUS risk score, n (%)					
0 (low)	16 (38)				
1 (intermediate-low)	20 (48)	n.a.	*n.a.*	*n.a.*	*n.a.*
2 (intermediate-high)	5 (12)				
3 (high)	1 (2)				
SMM 20/2/20 risk score, n (%)					
0 (low)	*n.a.*	7	*n.a.*	*n.a.*	*n.a.*
1 (intermediate)		7			
≥2 (high)		8			
Immunoglobulin subtype, n (%)					*n.a.*

IgG	33 (78)	16 (73)	10 (67)	13 (54)	
IgA	4 (10)	5 (23)	4 (27)	6 (25)	
LCO	1 (2)	1 (4.5)	1 (7)	5 (21)	
IgM	4 (10)	0 (0)	0 (0)	0 (0)	
Induction treatment, n (%)					
PI				6 (25)	
IMiD	*n.a.*	*n.a.*	*n.a.*	3 (13)	*n.a.*
PI + IMiD				15 (62)	
Other				0 (0)	
HD/ASCT					
No HD/ASCT	*n.a.*	*n.a.*	*n.a.*	7 (29)	*n.a.*
Single HD/ASCT				12 (50)	
Tandem HD/ASCT				5 (21)	
Treatment at sampling, n (%)					
IMiD				19 (79)	
Anti-CD38	*n.a.*	*n.a.*	*n.a.*	0 (0)	*n.a.*
Anti-CD38 + IMiD				0 (0)	
Anti-BCMA CAR-T				1 (4)	
watch and wait				4 (17)	
Remission at sampling, n (%)					
complete response (CR)	*n.a.*	*n.a.*	initial diagnosis	17 (71)	*n.a.*
partial response (PR)				4 (17)	
progressive disease (PD)				3 (12)	

** Samples were obtained from a blood bank and were fully anonymized.*

FIGURE LEGENDS

Figure 1. Overview of study design and samples. The study included five cohorts: healthy individuals, monoclonal gammopathy of undetermined significance (MGUS), smouldering multiple myeloma (SMM), newly diagnosed MM (NDMM), and treated MM. Peripheral blood mononuclear cells (PBMC) were collected from all participants, and six additional matched bone marrow (BM) aspirates were obtained. After quality control, samples were analysed by multi-dimensional multicolour flow cytometry to characterise $CD56^+$ circulating tumour plasma cell (CTPC) phenotypes. Created with BioRender.com.

Figure 2. Distribution of B cell subsets in peripheral blood changes with disease evolution. (A) Proportion of B cells ($CD19^+$) among $CD45^+$ peripheral blood cells for each group; n(Healthy)=9; n(MGUS)= 42; n(SMM)=22; n(NDMM)=15. Whiskers mark min and max. **(B)** Distribution of B cell subsets according to disease stage. Values are shown as percentage of total B cells in PB. Statistical significance was determined via ANOVA or Kruskal Wallis with post hoc FDR correction. Asterisks mark a statistically significant discovery.

Figure 3. $CD56^+$ CTPC counts discriminate disease stage. (A) Relative distribution of $CD56^-$ circulating plasma cells ($CD45^-$ $CD38^+$ $CD56^-$) for each group; n(Healthy)=10, n(MGUS)=42, n(SMM)=22, n(NDMM)=15. **(B)** Relative distribution of $CD56^+$ circulating tumour plasma cells (CTPCs, $CD45^-$ $CD38^+$ $CD56^+$) for each group. **(C)** Percentage of $CD56^+$ CTPCs from all CPCs for each group. Data is presented as box-and-whisker plot with median values indicated. Statistical significance was determined via Welch's ANOVA with post hoc FDR correction. Asterisks mark a statistically significant discovery. **(D)** Visualization of the distribution of „CTPC high" samples ($\geq$ 0.02% $CD56^+$ CTPCs of all nucleated cells in PB) vs „CTPC low" samples (< 0.02% $CD56^+$ CTPCs) at different disease stages.

Figure 4. **$CD56^+$ CTPCs show phenotypic evolution and expression of atypical markers with disease progression. (A-F)** Expression of surface markers within the $CD56^+$ CTPC population at different disease stages, displayed as heatmap; n(MGUS)=41, n(SMM)=22, n(NDMM)=15. Values are shown as change in the group mean MFI compared to the mean of the healthy control group (n=10). CPCs were used as control in the healthy cohort. **(G-J)** Transformed mean fluorescence intensity (MFI) values on $CD56^+$ CTPCs at different disease stages for CD45RA, CD123, PD1 and CCR7 in comparison to CPCs from the healthy cohort. Data is presented as box-and-whisker plots with median values indicated. Statistical significance was determined via ANOVA or Kruskal Wallis with post hoc FDR correction. Asterisks mark a statistically significant discovery, ns = no statistically significant discovery.

Figure 5. Comparison of expression patterns on $CD56^+$ CTPCs in untreated and treated MM. (A-F) Transformed mean fluorescence intensity (MFI) values of selected markers on $CD56^+$ CTPCs in treated and untreated MM; n(NDMM)=15, n(treated MM)=24. Data is presented as box-and-whisker plots with median values indicated. Statistical significance was determined via Welch's t-test (for normally distributed data) or Mann-Whitney test (for nonparametric data). * P <0.05, ** P <0.01, *** P <0.001, **** $P \leq 0.0001$

Figure 6. Comparison of paired bone marrow and peripheral blood samples in NDMM. (A-D) Transformed mean fluorescence intensity (MFI) values of selected markers on abnormal, $CD56^+$ PC in paired BM and PB samples (n=6). Paired samples are connected by a line.

Statistical significance was determined via paired t-test (for normally distributed data) or Wilcoxon test (for nonparametric data). * P <0.05, ** P <0.01, *** P <0.001.

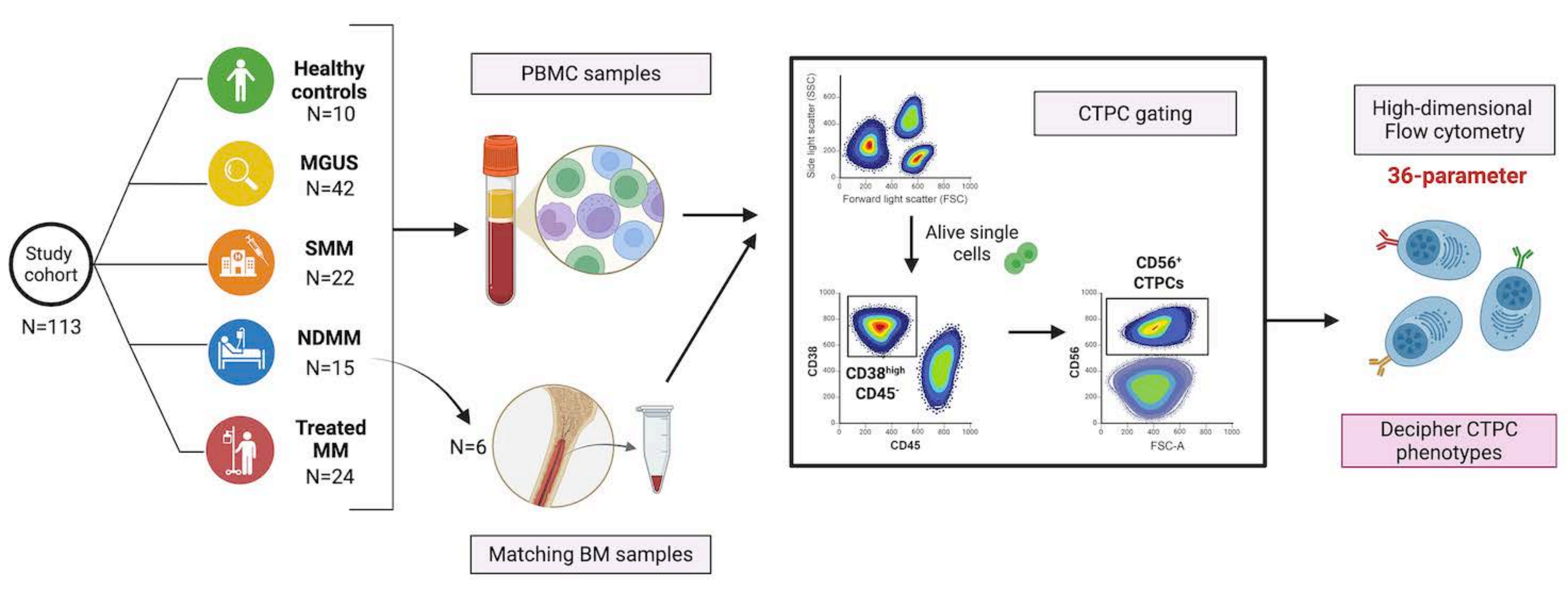
Study cohort
N=113
Healthy controls
N=10
MGUS
N=42
SMM
N=22
NDMM
N=15
Treated MM
N=24
PBMC samples
N=6
Matching BM samples
CTPC gating
Side light scatter (SSC)
Forward light scatter (FSC)
Alive single cells
CD38
CD45
CD38high CD45-
CD56+ CTPCs
CD56
FSC-A
High-dimensional Flow cytometry
36-parameter
Decipher CTPC phenotypes

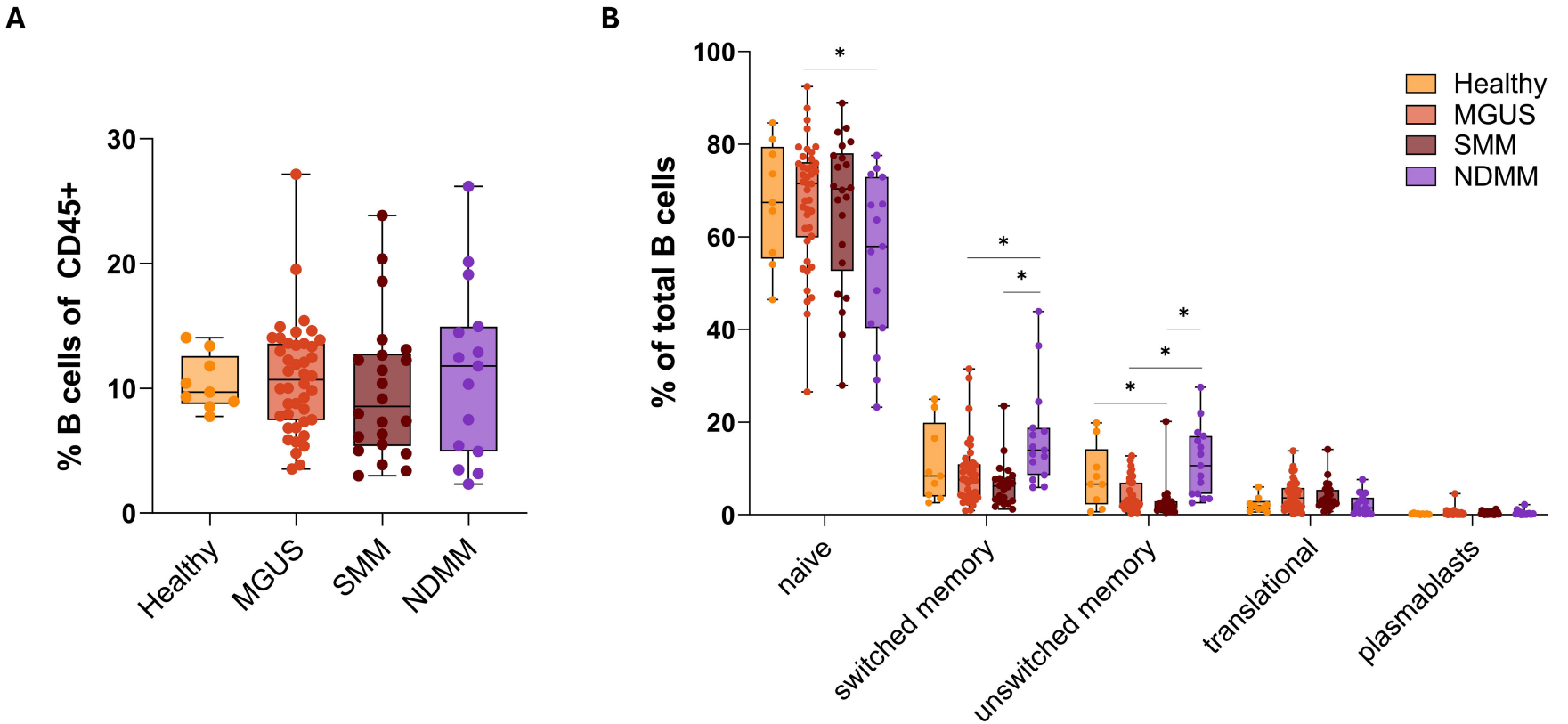
A
% B cells of CD45+
30
20
10
0
Healthy
MGUS
SMM
NDMM
B
% of total B cells
100
80
60
40
20
0
*
naive
switched memory
unswitched memory
translational
plasmablasts
Healthy
MGUS
SMM
NDMM

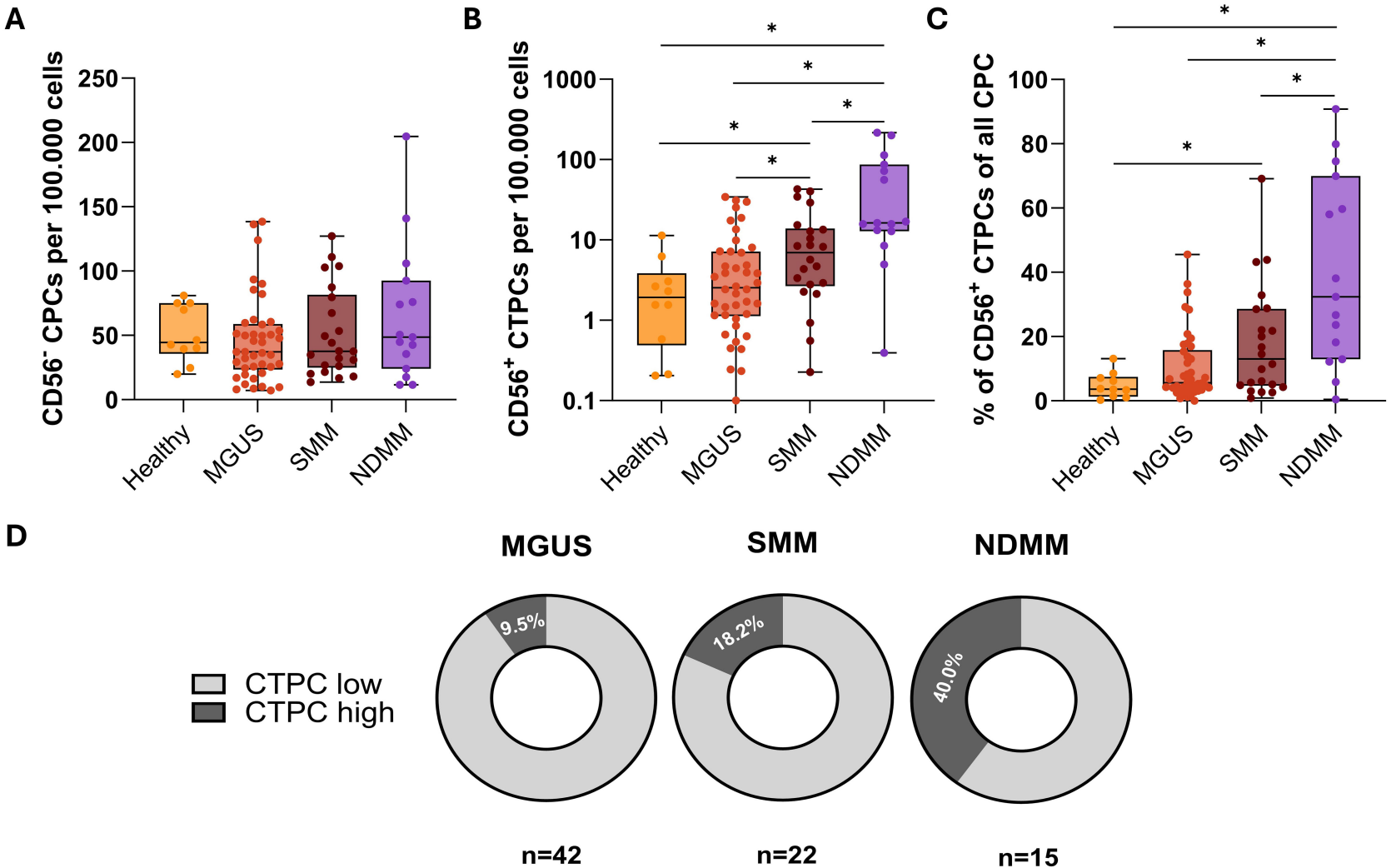
A
CD56- CPCs per 100.000 cells
250
200
150
100
50
0
Healthy
MGUS
SMM
NDMM
B
CD56+ CTPCs per 100.000 cells
1000
100
10
1
0.1
*
C
% of CD56+ CTPCs of all CPC
100
80
60
40
20
0
D
MGUS
SMM
NDMM
CTPC low
CTPC high
9.5%
18.2%
40.0%
n=42
n=22
n=15

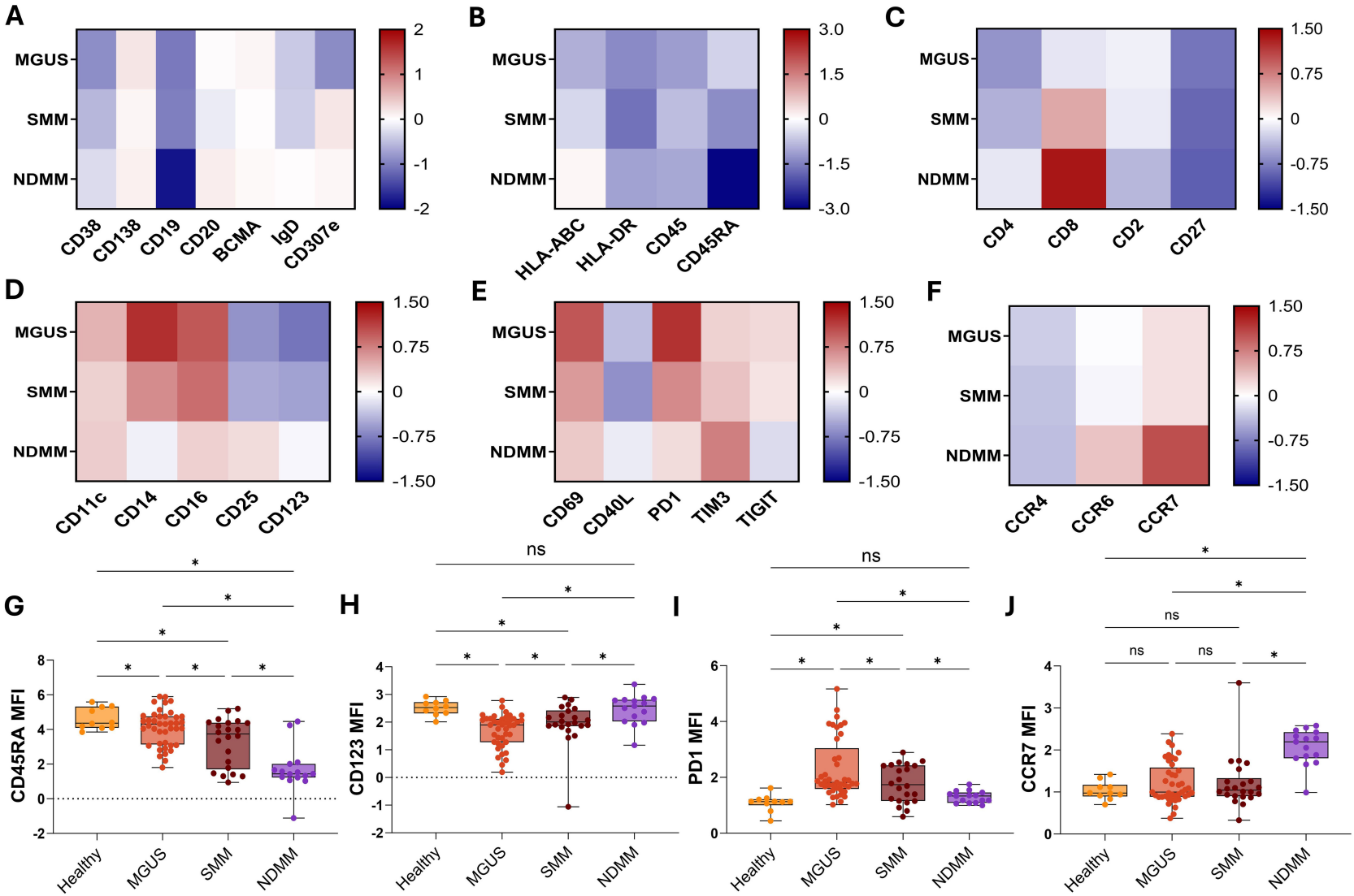
A
MGUS
SMM
NDMM
CD38
CD138
CD19
CD20
BCMA
IgD
CD307e
2
1
0
-1
-2
B
HLA-ABC
HLA-DR
CD45
CD45RA
3.0
1.5
0
-1.5
-3.0
C
CD4
CD8
CD2
CD27
1.50
0.75
0
-0.75
-1.50
D
CD11c
CD14
CD16
CD25
CD123
E
CD69
CD40L
PD1
TIM3
TIGIT
F
CCR4
CCR6
CCR7
G
CD45RA MFI
H
CD123 MFI
I
PD1 MFI
J
CCR7 MFI
Healthy
ns
*

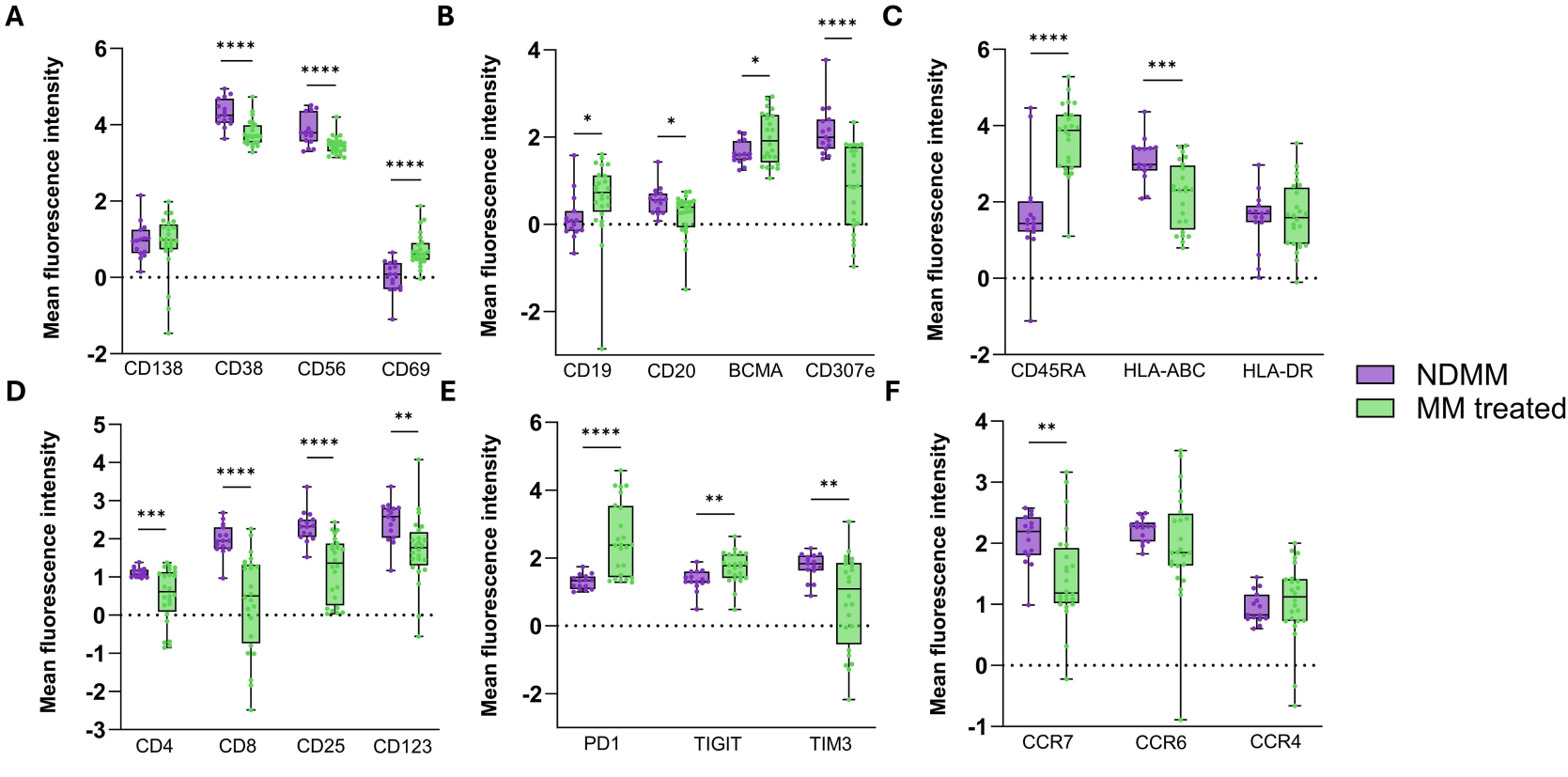
A
B
C
D
E
F
Mean fluorescence intensity
CD138
CD38
CD56
CD69
CD19
CD20
BCMA
CD307e
CD45RA
HLA-ABC
HLA-DR
CD4
CD8
CD25
CD123
PD1
TIGIT
TIM3
CCR7
CCR6
CCR4
NDMM
MM treated

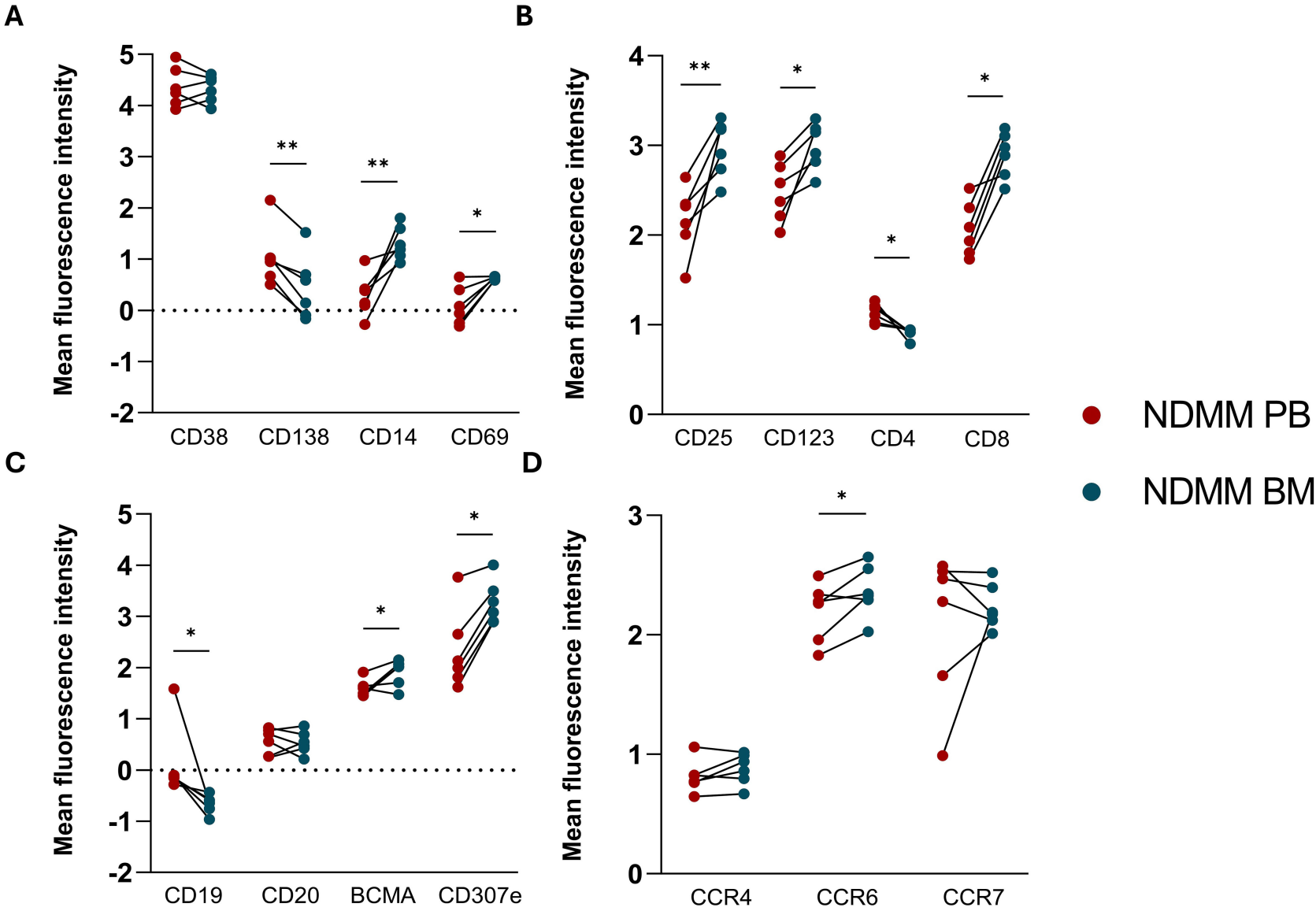
A
Mean fluorescence intensity
5
4
3
2
1
0
-1
-2
**
**
*
CD38
CD138
CD14
CD69
B
Mean fluorescence intensity
4
3
2
1
0
**
*
*
*
CD25
CD123
CD4
CD8
C
Mean fluorescence intensity
5
4
3
2
1
0
-1
-2
*
*
*
CD19
CD20
BCMA
CD307e
D
Mean fluorescence intensity
3
2
1
0
*
CCR4
CCR6
CCR7
NDMM PB
NDMM BM

Supplementary Information to

"Phenotypic evolution of circulating plasma cells from early precursor stages to multiple myeloma"

Martin Pietzsch[1]*, Sina Alexandra Beer[1]*, Lucca Marco Kimmich[1], Chiara Windsor[1], Sarah Gekeler[1], Britta Besemer[1], Anna Maria Paczulla Stanger[1,2]

Author affiliations:
[1] University Clinic Tübingen, Department for Internal Medicine II, University of Tübingen, Tübingen, Germany

[2] Flow Cytometry Core Facility, Medical Faculty Tübingen, University of Tübingen, Tübingen, Germany

* These authors contributed equally to this work and share first authorship.

Supplementary information on methodology

Study population: exclusion criteria

HIV- or hepatitis C infections were exclusion criteria in patients and healthy donors. Patients with monoclonal gammopathy of clinical significance, amyloidosis or patients with additional hematologic malignancies were also excluded.

Patient samples

Peripheral blood mononuclear cells (PBMCs) were enriched by density gradient centrifugation (Sepmate, StemCell Technologies according to manufacturer's protocol and Pancoll, Pan-Biotech) and viably frozen in RPMI1640 medium (ThermoFisher) supplemented with 20% fetal bovine serum (FBS) and 10% DMSO (AppliChem).

Analysis of Multiparameter spectral flow-cytometry.

All datasets were processed using the Cytolution software platform (from Cytolytics GmbH), which implements a flexible pipeline consisting of data preprocessing followed by downstream analytical workflows. The pipeline is designed to standardize data quality, reduce technical variability, and ensure robust performance of downstream algorithms. Signal intensities were transformed on a per-channel basis using an inverse hyperbolic sine (asinh) transformation: $ft(x)=asinh((x-Poffset)/Pwidth)$.

Transformation parameters (Poffset and Pwidth) were estimated running an algorithmic optimization procedure. Scatter parameters were excluded from asinh transformation and instead scaled linearly, while the time channel was excluded entirely. All transformation parameters were retained and made available for inspection or manual adjustment.

To mitigate systematic technical variation across samples, a batch correction step was applied. The effectiveness of batch correction was evaluated using pre- and post-correction

visualizations, allowing assessment of residual batch effects and potential overcorrection. For analysis of marker expression according to their respective MFI, semi-automated cluster exploring was applied.

Flow Cytometry Antibodies

All anti-human antibodies were titrated to determine the optimal concentration prior to the staining of patient samples. For this purpose, cell line LP-1 (ACC 41, RRID:CVCL_0012) was obtained from DSMZ and tested negative for mycoplasma contamination, moreover PBMCs were used. Antibodies and viability dye were purchased from either BioLegend (BL), BD Biosciences (BD), ThermoFisher Scientific (Thermo), or Novus Biologicals (Novus) under the following catalog numbers: CD45 (BL, #304026, RRID:AB_893337), CD3 (BD, #750981, RRID:AB_2875050), TCRγδ (BD, #655410, RRID:AB_2870377), CD45RA (BD, #740806, RRID:AB_2740469), CCR7 (BL, #353264, RRID:AB_2894483), CD56 (BD, #749086, RRID:AB_2873478), CD16 (BL, #302068, RRID:AB_2876587), CD14 (Thermo, #H007T02B05, RRID:AB_3098075), HLA-DR (BD, #564231, RRID:AB_2738685), HLA-ABC (BL, #311406, RRID:AB_314875), CD19 (BD, #567344, RRID:AB_2916561), CD11c (BL, #301628, RRID:AB_11203895), CD123 (BL, #306012, RRID:AB_439779), CD20 (BL, #302332, RRID:AB_2563805), IgD (BD, #741394, RRID:AB_2870889), CD27 (Thermo, #46-0279-41, RRID:AB_1834392), CD38 (BD, #612970, RRID:AB_2916888), CD138 (BL, #356548, RRID:AB_2894487), BCMA (BL, #357528, RRID:AB_2890787), CD8 (BD, #741199, RRID: AB_2870759), CD2 (BD, #745205, RRID: AB_3684781), CD4 (BL, #344672, RRID: AB_2894479), CCR6 (BD, #612780, RRID: AB_2870109), CD307e (BD, #749606, RRID: AB_2873908), CCR4 (BL, #359436, RRID: AB_2894491), CXCR3 (BL, #353714, RRID: AB_10962908), CD25 (BL, #302618, RRID: AB_493045), TIGIT (BL, #372734, RRID: AB_2876700), PD-1 (Thermo, #62-2799-42, RRID: AB_2784827), TIM-3 (BD, #752363, RRID: AB_2875880), CD40L (BL, #310842, RRID: AB_2572187), CD127 (BD, #742547, RRID: AB_2740857), CD69 (Novus, #NBP1-43387AF532, RRID: AB_3209264), LIVE/DEAD™ Fixable Blue Dead Cell Staining dye (Thermo, #L34961).

Statistics

Effect sizes included eta squared/η^2 (one-way ANOVA), epsilon squared/ε^2 (Welch/Brown–Forsythe ANOVA and K-W), d_z (paired t-tests), Hedges' g_w (Welch's t-test) and r_{rb} (Mann–Whitney U), with 95% confidence intervals where applicable.

Supplementary Figures

Supplementary Figure 1. Gating Strategy for the identification of CD56^{+} circulating tumour plasma cells (CTPCs).

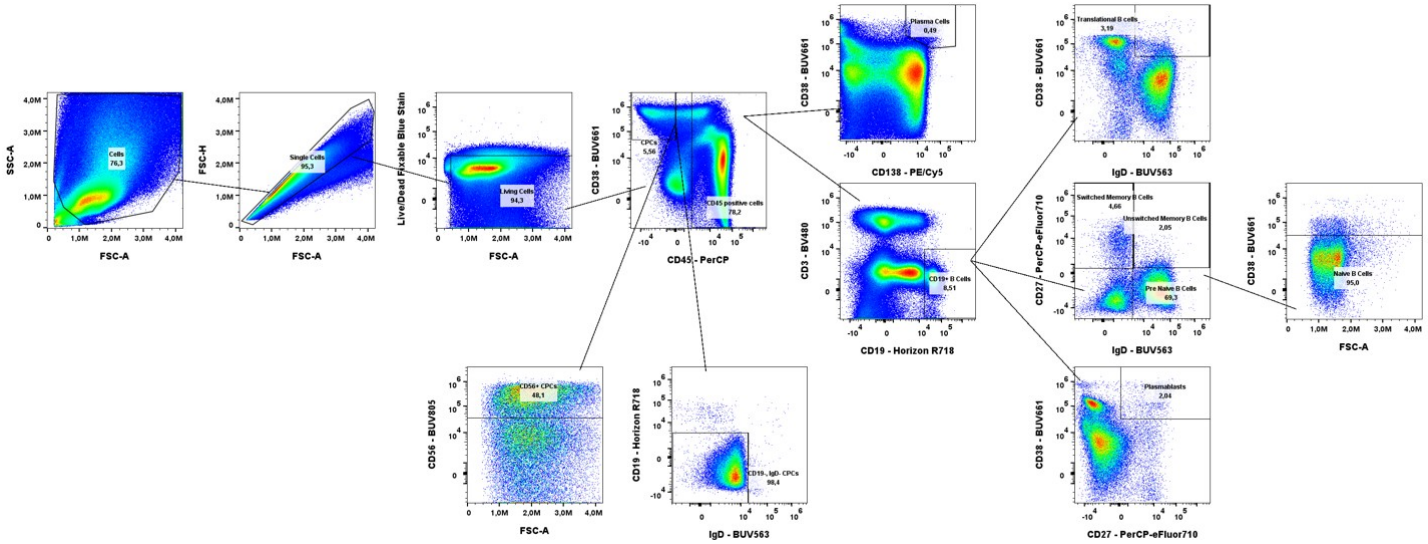

Supplementary Figure 2. Additional boxplots of each marker across disease stages. Transformed mean fluorescence intensity (MFI) values on $CD56^{+}$ CTPCs at different disease stages. Data is presented as box-and-whisker plot with median values indicated. Statistical significance was determined via ANOVA or Kruskal Wallis with post hoc FDR correction. Asterisks mark a statistically significant discovery, ns = no statistically significant discovery.

Supplementary Figure 3. Paired dot-plots of each marker comparing peripheral blood and bone marrow samples. Transformed mean fluorescence intensity (MFI) values (Y-axis) of markers on abnormal, $CD56^{+}$ PC in paired BM and PB samples. Paired samples are connected by a line. Statistical significance was determined via paired t-test (for normally distributed data) or Wilcoxon test (for nonparametric data). * P <0.05, ** P <0.01, *** P <0.001.

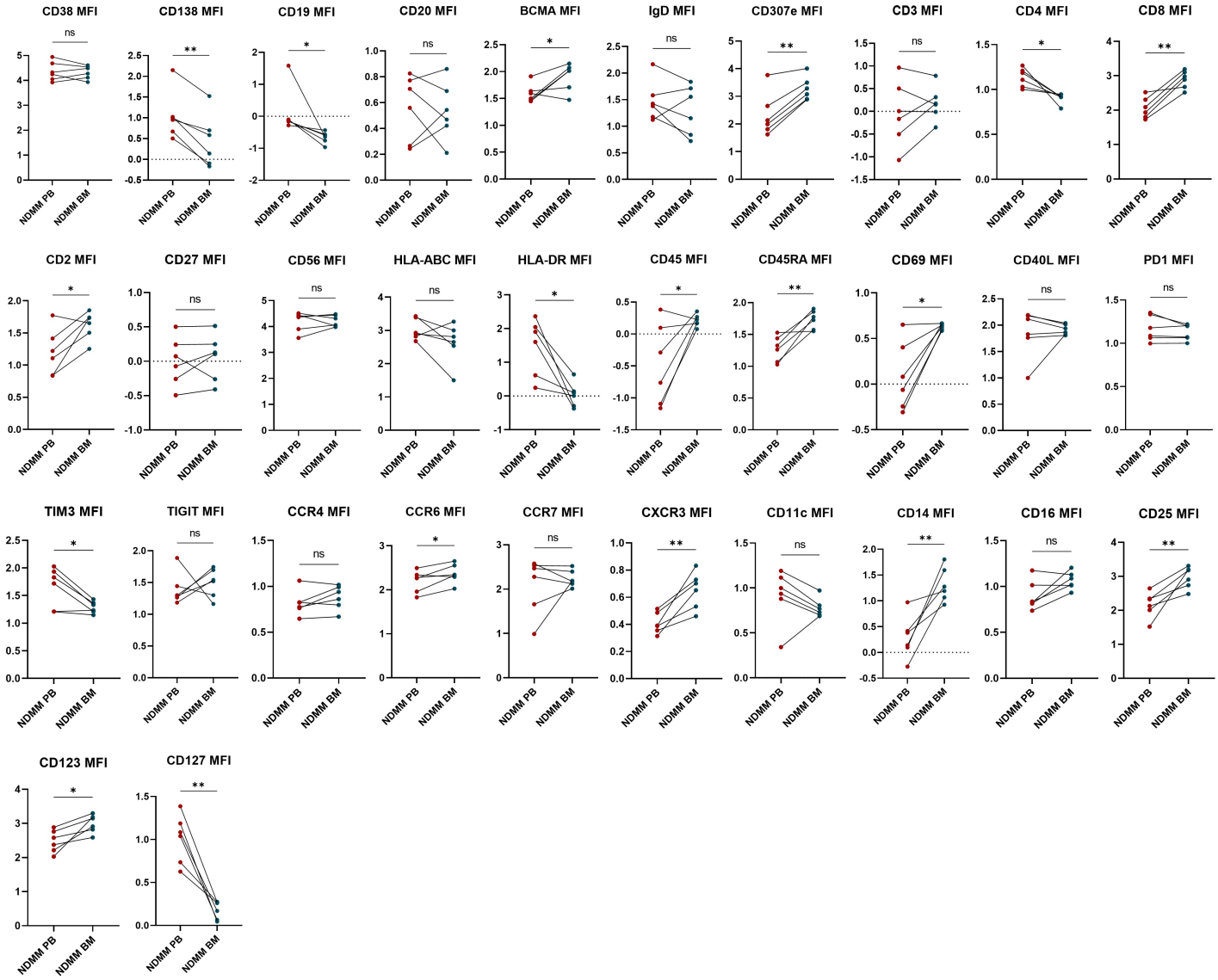

Supplementary Figure 4. Exemplary gating of a newly diagnosed multiple myeloma (NDMM) sample. The figure shows the gating strategy for circulating plasma cells (CPCs), followed by analysis of CD56 and CD45RA expression. Lineage marker expression is presented as histograms with overlays depicting the expression on B cells, T cells, and CD56^{+} circulating tumour plasma cells (CTPCs).

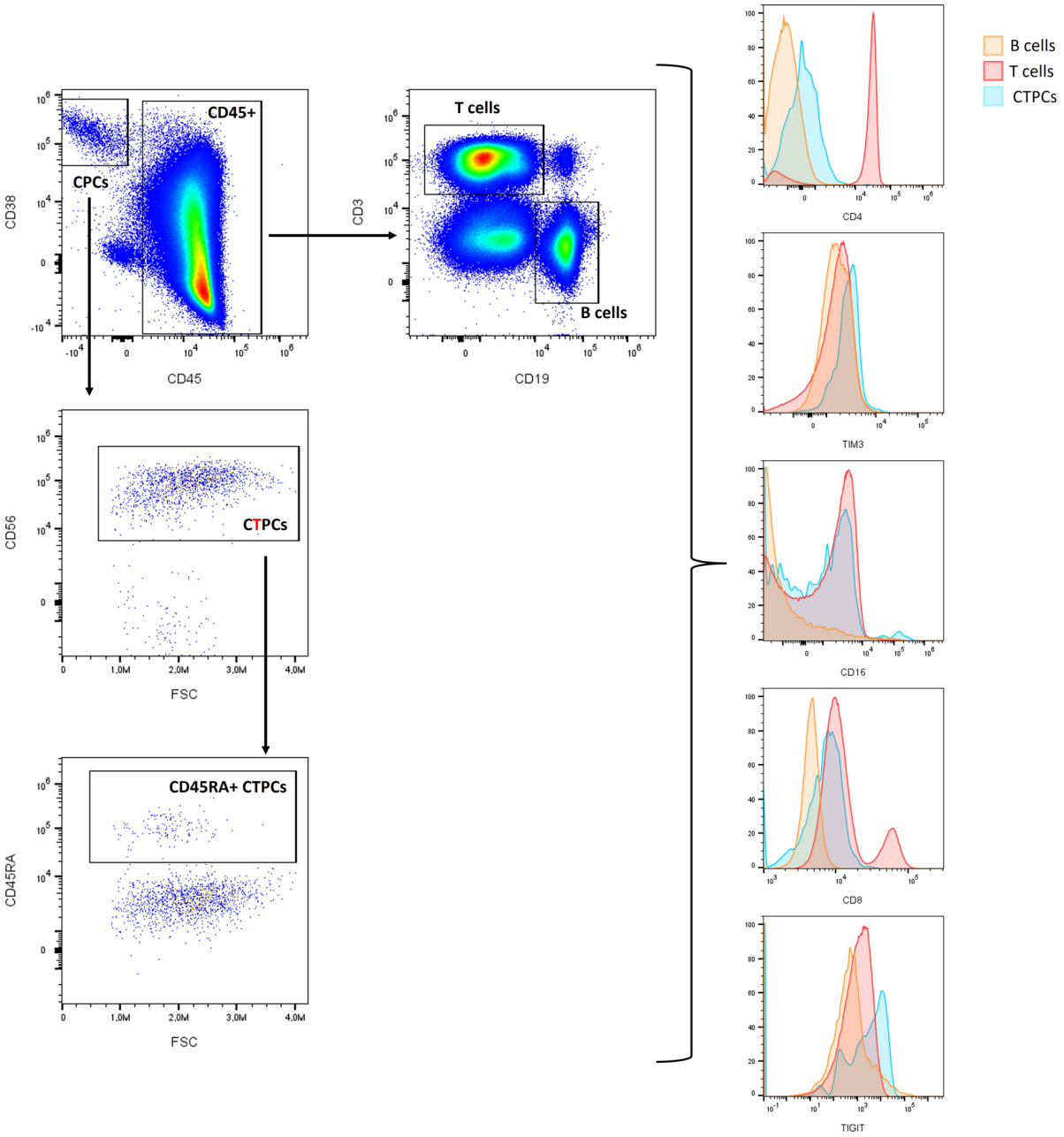

Supplementary Tables

Supplementary Table 1. Overview of the applied antibodies for the study. For each antibody, clone, providing company, and fluorophore are shown. All antibodies have been titrated on respective antigen-expressing control cells prior to the staining of patient cells.

Antigen	Clone	Fluorophor	Company	Catalog No.
CD45	HI30	PerCP*	BioLegend	304026
CD3	OKT3	BV480	BD Biosciences	750981
TCR γδ	B1	PE-Cy7	BD Biosciences	655410
CD45RA	5H9	BV711	BD Biosciences	740806
CCR7	G043H7	APC-Fire 810	BioLegend	353264
CD56	NCAM16.2	BUV805	BD Biosciences	749086
CD16	3G8	PE-Fire 640	BioLegend	302068
CD14	MEM-15	NovaFlour Blue610	ThermoFisher	H007T02B05
HLA-DR	G46-6	BV650	BD Biosciences	564231
HLA-ABC	w6/32	PE	BioLegend	311406
CD19	HIB19	Horizon R718	BD Biosciences	567344
CD11c	3.9	BV421	BioLegend	301628
CD123	6H6	APC	BioLegend	306012
CD20	2H7	BV570	BioLegend	302332
IgD	IA62	BUV563	BD Biosciences	741394
CD27	O323	PerCP-e Fluor 710	ThermoFisher	46-0279-41
CD38	HIT2	BUV661	BD Biosciences	612970
CD138	MI15	PE-Cy5	BioLegend	356548
BCMA	19F2	KIRAVIA Blue 520	BioLegend	357528
CD8	SK1	BUV496	BD Biosciences	741199
CD2	S5.2	BV605	BD Biosciences	745205
CD4	SK3	Spark YG 593	BioLegend	344672
CCR6	11A9	BUV737	BD Biosciences	612780
CD307e	509F6	BV510	BD Biosciences	749606
CCR4	L291H4	PE-Fire 700	BioLegend	359436
CXCR3	G025H7	PerCP-Cy5.5	BioLegend	353714
CD25	BC96	AF647	BioLegend	302618
TIGIT	A15153G	APC-Cy7	BioLegend	372734
PD-1	J105	Super Bright 436	ThermoFisher	62-2799-42

TIM-3	7D3	BUV615	BD Biosciences	752363
CD40L	24-31	BV785	BioLegend	310842
CD127	HIL-7R-M21	BUV395	BD Biosciences	742547
CD69	FN50	Alexa Fluor 532	Novus Biologicals	NBP1-43387AF532
LIVE/DEAD™ Fixable Blue Dead Cell Staining dye	-	-	ThermoFisher	L34961

Supplementary Table 2. Differential expression of CTPC surface markers across disease stages. Overall *P*-values are shown for group comparisons, with pairwise comparisons between healthy controls, MGUS, SMM, and NDMM provided with adjusted *P*-values. Adjusted *P*-values < 0.05 are marked in bold.

Marker	Overall *P*	Comparison	q / adjusted *P*
CD38	**<0.001**	**Healthy vs. MGUS** **Healthy vs. SMM** Healthy vs. NDMM **MGUS vs. SMM** **MGUS vs. NDMM** **SMM vs. NDMM**	**<0.001** **0.004** 0.083 **0.004** **<0.001** **0.048**
CD138	0.712	Healthy vs. MGUS Healthy vs. SMM Healthy vs. NDMM MGUS vs. SMM MGUS vs. NDMM SMM vs. NDMM	0.965 >0.999 >0.999 0.965 0.965 >0.999
CD19	**<0.001**	**Healthy vs. MGUS** **Healthy vs. SMM** **Healthy vs. NDMM** MGUS vs. SMM **MGUS vs. NDMM** **SMM vs. NDMM**	**<0.001** **<0.001** **<0.001** 0.099 **<0.001** **<0.001**
CD20	0.087	Healthy vs. MGUS Healthy vs. SMM Healthy vs. NDMM MGUS vs. SMM MGUS vs. NDMM SMM vs. NDMM	0.993 0.340 0.633 0.169 0.510 0.100
BCMA	0.950	Healthy vs. MGUS Healthy vs. SMM Healthy vs. NDMM MGUS vs. SMM MGUS vs. NDMM	0.988 0.988 0.988 0.988 0.988

		SMM vs. NDMM	0.988
IgD	**<0.001**	**Healthy vs. MGUS**	**<0.001**
		Healthy vs. SMM	**0.003**
		Healthy vs. NDMM	0.236
		MGUS vs. SMM	0.102
		MGUS vs. NDMM	**<0.001**
		SMM vs. NDMM	**0.003**
CD307e	**<0.001**	Healthy vs. MGUS	0.101
		Healthy vs. SMM	0.464
		Healthy vs. NDMM	0.123
		MGUS vs. SMM	**0.005**
		MGUS vs. NDMM	**<0.001**
		SMM vs. NDMM	0.133
CD3	**0.006**	Healthy vs. MGUS	0.279
		Healthy vs. SMM	0.830
		Healthy vs. NDMM	0.174
		MGUS vs. SMM	0.215
		MGUS vs. NDMM	**0.002**
		SMM vs. NDMM	0.098
CD4	**0.002**	**Healthy vs. MGUS**	**0.003**
		Healthy vs. SMM	**0.011**
		Healthy vs. NDMM	0.196
		MGUS vs. SMM	0.327
		MGUS vs. NDMM	**0.014**
		SMM vs. NDMM	0.051
CD8	**<0.001**	Healthy vs. MGUS	0.083
		Healthy vs. SMM	**0.010**
		Healthy vs. NDMM	**<0.001**
		MGUS vs. SMM	**0.031**
		MGUS vs. NDMM	**<0.001**
		SMM vs. NDMM	**<0.001**
CD2	0.144	Healthy vs. MGUS	0.943
		Healthy vs. SMM	0.943
		Healthy vs. NDMM	0.268
		MGUS vs. SMM	0.943
		MGUS vs. NDMM	0.138
		SMM vs. NDMM	0.268
CD27	**<0.001**	**Healthy vs. MGUS**	**<0.001**
		Healthy vs. SMM	**<0.001**
		Healthy vs. NDMM	**<0.001**
		MGUS vs. SMM	0.341
		MGUS vs. NDMM	0.196
		SMM vs. NDMM	0.313
HLA-ABC	**<0.001**	**Healthy vs. MGUS**	**0.002**
		Healthy vs. SMM	0.099
		Healthy vs. NDMM	0.552
		MGUS vs. SMM	**0.034**
		MGUS vs. NDMM	**<0.001**
		SMM vs. NDMM	**0.038**
HLA-DR	**<0.001**	**Healthy vs. MGUS**	**<0.001**
		Healthy vs. SMM	**<0.001**
		Healthy vs. NDMM	**0.009**
		MGUS vs. SMM	0.185

		MGUS vs. NDMM	0.127
		SMM vs. NDMM	**0.047**
CD45	**<0.001**	**Healthy vs. MGUS**	**<0.001**
		Healthy vs. SMM	**0.002**
		Healthy vs. NDMM	**<0.001**
		MGUS vs. SMM	**0.007**
		MGUS vs. NDMM	0.134
		SMM vs. NDMM	0.099
CD45RA	**<0.001**	**Healthy vs. MGUS**	**0.034**
		Healthy vs. SMM	**<0.001**
		Healthy vs. NDMM	**<0.001**
		MGUS vs. SMM	**0.002**
		MGUS vs. NDMM	**<0.001**
		SMM vs. NDMM	**<0.001**
CD69	**<0.001**	**Healthy vs. MGUS**	**<0.001**
		Healthy vs. SMM	**0.003**
		Healthy vs. NDMM	0.144
		MGUS vs. SMM	**0.017**
		MGUS vs. NDMM	**<0.001**
		SMM vs. NDMM	**0.014**
CD40L	**0.001**	Healthy vs. MGUS	0.071
		Healthy vs. SMM	0.638
		Healthy vs. NDMM	**0.005**
		MGUS vs. SMM	**0.040**
		MGUS vs. NDMM	**0.040**
		SMM vs. NDMM	**0.002**
PD1	**<0.001**	**Healthy vs. MGUS**	**<0.001**
		Healthy vs. SMM	**0.002**
		Healthy vs. NDMM	0.126
		MGUS vs. SMM	**0.036**
		MGUS vs. NDMM	**<0.001**
		SMM vs. NDMM	**0.011**
TIM3	**0.023**	Healthy vs. MGUS	0.093
		Healthy vs. SMM	0.103
		Healthy vs. NDMM	**0.012**
		MGUS vs. SMM	0.589
		MGUS vs. NDMM	0.103
		SMM vs. NDMM	0.103
TIGIT	**0.004**	Healthy vs. MGUS	0.119
		Healthy vs. SMM	0.257
		Healthy vs. NDMM	0.257
		MGUS vs. SMM	0.289
		MGUS vs. NDMM	**0.002**
		SMM vs. NDMM	**0.027**
CCR4	**0.031**	**Healthy vs. MGUS**	**0.024**
		Healthy vs. SMM	**0.011**
		Healthy vs. NDMM	**0.011**
		MGUS vs. SMM	0.248
		MGUS vs. NDMM	0.248
		SMM vs. NDMM	0.437
CCR6	**0.007**	Healthy vs. MGUS	0.585
		Healthy vs. SMM	0.585
		Healthy vs. NDMM	0.050

		MGUS vs. SMM	0.665
		MGUS vs. NDMM	**0.004**
		SMM vs. NDMM	**0.005**
CCR7	**<0.001**	Healthy vs. MGUS	0.341
		Healthy vs. SMM	0.341
		Healthy vs. NDMM	**<0.001**
		MGUS vs. SMM	0.488
		MGUS vs. NDMM	**<0.001**
		SMM vs. NDMM	**<0.001**
CXCR3	0.534	Healthy vs. MGUS	0.718
		Healthy vs. SMM	0.718
		Healthy vs. NDMM	0.718
		MGUS vs. SMM	0.718
		MGUS vs. NDMM	0.718
		SMM vs. NDMM	0.718
CD11c	**0.008**	**Healthy vs. MGUS**	**0.003**
		Healthy vs. SMM	**0.037**
		Healthy vs. NDMM	**0.016**
		MGUS vs. SMM	0.209
		MGUS vs. NDMM	0.524
		SMM vs. NDMM	0.393
CD14	**0.010**	Healthy vs. MGUS	0.056
		Healthy vs. SMM	0.173
		Healthy vs. NDMM	0.777
		MGUS vs. SMM	0.386
		MGUS vs. NDMM	**0.021**
		SMM vs. NDMM	0.103
CD16	**0.001**	**Healthy vs. MGUS**	**0.003**
		Healthy vs. SMM	**0.007**
		Healthy vs. NDMM	0.206
		MGUS vs. SMM	0.382
		MGUS vs. NDMM	**0.011**
		SMM vs. NDMM	**0.033**
CD25	**<0.001**	**Healthy vs. MGUS**	**0.003**
		Healthy vs. SMM	**0.011**
		Healthy vs. NDMM	0.225
		MGUS vs. SMM	0.225
		MGUS vs. NDMM	**<0.001**
		SMM vs. NDMM	**<0.001**
CD123	**<0.001**	**Healthy vs. MGUS**	**<0.001**
		Healthy vs. SMM	**0.007**
		Healthy vs. NDMM	0.220
		MGUS vs. SMM	**0.038**
		MGUS vs. NDMM	**<0.001**
		SMM vs. NDMM	**0.010**
CD127	**<0.001**	**Healthy vs. MGUS**	**0.008**
		Healthy vs. SMM	**0.071**
		Healthy vs. NDMM	**<0.001**
		MGUS vs. SMM	0.068
		MGUS vs. NDMM	**0.006**
		SMM vs. NDMM	**<0.001**
CD56	**<0.001**	**Healthy vs. MGUS**	**<0.001**
		Healthy vs. SMM	**<0.001**

		Healthy vs. NDMM **MGUS vs. SMM** **MGUS vs. NDMM** SMM vs. NDMM	**<0.001** **0.037** **0.003** 0.081